RSC Advances

PAPER

View Article Online
View Journal | View Issue

Cite this: *RSC Adv.*, 2026, **16**, 3725

Nano-$NiCo_2O_4$-catalyzed dehydrogenative direct esterification and amidation of primary alcohols under microwave conditions

Kumari Anchal,[a] Keya Roy,[b] Laksmikanta Adak*[b] and Subhash Banerjee *[a]

Here, we demonstrate $NiCo_2O_4$ nanoparticle-catalyzed dehydrogenative esterification and amidation of primary alcohols to esters of fatty acids and amides under microwave irradiation, without the need for any oxidant, achieving excellent yields of esters (50–92%) and amides (72–80%). The $NiCo_2O_4$ nanomaterial was prepared through co-precipitation, and its composition, morphology, structure, and textural properties were analyzed *via* powder XRD, FESEM, EDX, TEM, and BET. The crystallite size was found to be 121.69 nm using the Scherrer equation, by considering the FWHM of the (311) diffraction plane. The FESEM and EDS analysis revealed the formation of spherical-shaped granules with a mean size of 0.251 μm and their elemental composition. Furthermore, HRTEM images with a mean size of 2.25 nm confirmed the formation of spherical $NiCo_2O_4$ nanoparticles. The mesoporous nature of the material is analyzed by the BET surface area (33.81 m^2 g^{-1}) and average pore diameter 23.49 nm. The $NiCo_2O_4$ nanoparticles remained stable throughout the reaction process and were reusable for up to eight cycles. The catalytic nature of $NiCo_2O_4$ has been proved by cyclic voltametric studies of fresh and recycled catalysts. The present dehydrogenative esterification and amidation protocol offers several advantages, for example, robust and recyclable $NiCo_2O_4$ nanoparticles as a catalyst, oxidant- and solvent-free reaction conditions, microwave-assisted faster reaction rate, excellent isolated yields of products, *etc.*

Received 24th September 2025
Accepted 3rd January 2026

DOI: 10.1039/d5ra07245j

rsc.li/rsc-advances

1 Introduction

The direct oxidation of primary alcohols to their corresponding esters or amides is one of the most important transformations, providing a straightforward method for accessing key functional groups. Esters represent a versatile class of organic compounds widely employed as solvents, key constituents in perfumes, essential oils, cosmetics, fuels, *etc.*[1–4] Amides are another significant derivative of carboxylic acids, widely used in the synthesis of fiber, lubricants, wax additives, plasticizers,[5] nylons, and as organic solvents. Furthermore, esters and amides have numerous applications in the pharmaceutical industry. The structures of a few pharmaceutically esters and amides are provided in Fig. 1. They are used as painkillers[6–8] (*e.g.*, Demerol,[6] Salsalate,[7] Phenacetin[8]), antiseptic agents[9] (*e.g.*, Lintrin), anti-inflammatory drugs[9] (*e.g.*, Acetylsalol), anesthetics[10,11] (*e.g.*, Procaine, [10] Benzocaine[11]), CNS stimulants[12] (*e.g.*, Methylphenidate), antiepileptic drugs[13] (*e.g.*, Levetiracetam), and immunomodulatory drugs[14] (*e.g.*, Teriflunamide). Conventionally, esters and amides are synthesized by the reactions of carboxylic acids or their derivatives with alcohols or amines using a strong acid as a catalyst.[15a] In this conventional route, carboxylic acid or its derivatives undergo activation followed by nucleophilic substitution at the acyl centre, typically promoted by strong Brønsted or Lewis acids. These methods

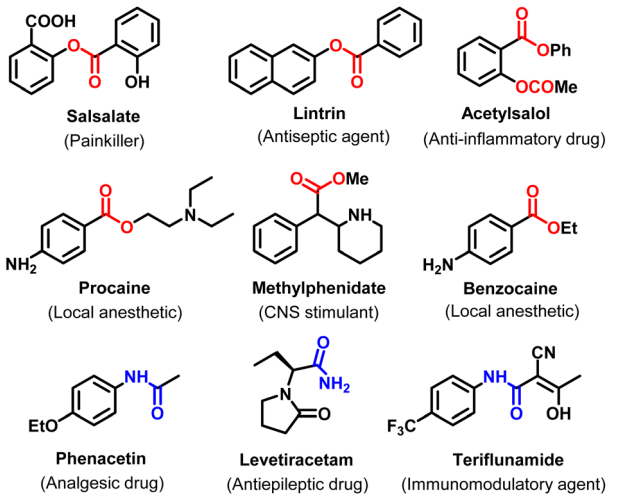

Fig. 1 Applications of esters and amides in the pharmaceutical industry.

[a]*Department of Chemistry, Guru Ghasidas Vishwavidyalaya, Koni, Bilaspur-495009, Chhattisgarh, India. E-mail: ocsb2006@gmail.com*

[b]*Department of Chemistry, Indian Institute of Engineering Science and Technology, Shibpur, Botanic Garden, Howrah 711103, India*

require hazardous reagents like acyl chlorides, anhydrides, and strong acids, which present significant handling risks. Additionally, the reaction occurs at elevated temperatures.

Moreover, the subsequent neutralization steps and formation of salt wastes significantly reduce the overall atom economy, making these transformations less attractive from an environmental standpoint.

To overcome the above limitations, transition metal-catalyzed direct oxidative as well as dehydrogenative esterification have been developed in the context of green synthesis. The direct oxidative esterification of alcohols[15b] typically proceeds as follows: in the initial step, the alcohol forms an alkoxy species in the presence of reactive oxygen species on the catalytic metal surface. This alkoxy species is then dehydrogenated to give an aldehyde. Subsequently, a hemiacetal forms by the reaction of the aldehyde with the alkoxy species. Further, an ester is formed by dehydrogenation of the hemiacetal group. In these pathways, there is a high reliance on an external oxidant. Additionally, these methods often produce unnecessary side reactions. The direct oxidative esterification has been carried out by using palladium,[16–20] ruthenium,[21–26] gold,[27–31] and iridium[32]-based catalysts. Alternatively, direct dehydrogenative esterification has been reported using Pyridine-based PNNH–Ru Pincer complexes,[33] [(^{iPr}PPPN^{Me}Py^{Me})CoCl]OTf,[34] [Cp*RhCl$_2$]2,[35a] Mn(^{Ph}PNN)(CO)$_2$Br,[35b] Dicationic Cp*Ir complex,[35c] Pt/SnO$_2$.[36]

On the other hand, only a few reports using Ru-2-(di-*tert*-butylphosphinomethyl)-6-(diethylaminomethyl)pyridine pincer complex,[37] [Ru(*p*-cymene)Cl$_2$]$_2$ or [Ru(benzene)Cl$_2$]$_2$,[38] RuH$_2$(PPh$_3$)$_4$,[39] [Rh(trop$_2$N)(PPh3)],[40] (^{iPr}PNP)Fe(H)(CO) (^{iPr}PNP = N[CH$_2$CH$_2$(P^i Pr$_2$)]$_2$),[41] Mn-Pincer Complex,[42] and Ag/Al$_2$O$_3$-5,[43] catalytic systems are available for the direct dehydrogenative amidation of primary alcohols. The dehydrogenative esterification or amidation provides a cleaner and more efficient alternative to oxidative methods without the need for pre-functionalized substrates, reducing the use of oxidants, additives, and by-products, and improving atom economy. The evolution of hydrogen gas as the sole by-product further aligns this method with green chemistry principles. Dehydrogenation of alcohols produces an aldehyde intermediate, with the release of H$_2$. An alcohol attacks the intermediate to give hemiacetal species, which undergo further dehydrogenation to produce an ester. However, the above-mentioned catalytic oxidative and dehydrogenative esterification and amidation suffer limitations such as the use of homogeneous catalysts containing expensive and scarce palladium, ruthenium, gold, and iridium complexes that demand rigorous reaction control. These metals, in combination with reactive and toxic ligands, hazardous oxidants, auxiliary additives or co-catalysts, prolonged heating at elevated temperatures, as well as the use of inert atmospheres, restrict the practical applications. Furthermore, these catalysts often suffer from difficult recovery, poor recyclability, limited tolerance toward functional groups, and high catalyst loading, making them unsuitable for large-scale or industrial deployment.

Recently, spinel structures (AB$_2$O$_4$) with binary and ternary mixtures of metal oxides have been established as promising redox catalysts.[44] The presence of two mixed-valence metal

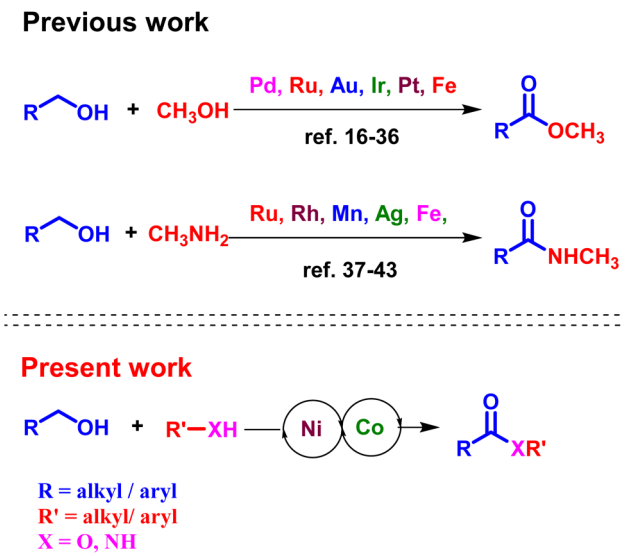

Scheme 1 Previous and present methods on esterification and amidation of primary alcohols.

cations provides an opportunity for the efficient transport of electrons between multiple transition-metal cations with a relatively low energy of activation. Among various transition metal oxides, spinel nickel cobaltite (NiCo$_2$O$_4$) benefits from the richer redox reactions of both nickel and cobalt ions, thus outperforming its components, nickel oxide and cobalt oxide.[45] It exhibits remarkable electrical conductivity and is widely used as a supercapacitor and a charge storage material.[45] As part of our continuous effort to explore the catalytic activities of heterogeneous nanocatalysts in organic transformations,[45g,46] we have taken the initiative to investigate the catalytic activities of metal cobaltite nanomaterials.[45g,46] Here, we report dehydrogenative oxidative esterification and amidation of primary alcohols using NiCo$_2$O$_4$ as a reusable catalyst, under solvent-free microwave conditions (Scheme 1). The major objective is to provide a scalable, environmentally benign pathway for the production of industrially relevant esters and amides *via* direct esterification and amidation of primary alcohols. The developed methodology eliminates the use of harmful additives or oxidants and operates under relatively mild conditions. Furthermore, the catalyst developed here is inexpensive, easy to fabricate, ligand-free, and heterogeneous, allowing convenient recovery and recyclability. These features enable the method to outperform previously reported methods and significantly enhance its overall practicality.

2 Materials and methods

2.1 Synthesis and characterization of NiCo$_2$O$_4$

Initially, we prepared NiCo$_2$O$_4$ by the co-precipitation method. Briefly, a 1000 mL beaker containing 500 mL of double-distilled water was heated, and then 20.0 mmol (4.7586 g) of cobalt chloride (CoCl$_2$·6H$_2$O) was added; the solution turned crimson red. Next, 10.0 mmol (1.295 g) of nickel chloride (NiCl$_2$) was added, and the resulting solution turned pink. Next, the sodium

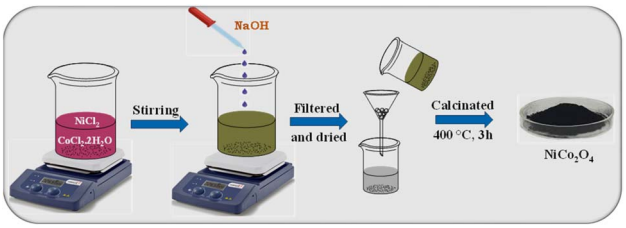

Scheme 2 Schematic illustration of the synthesis of $NiCo_2O_4$ *via* the co-precipitation method.

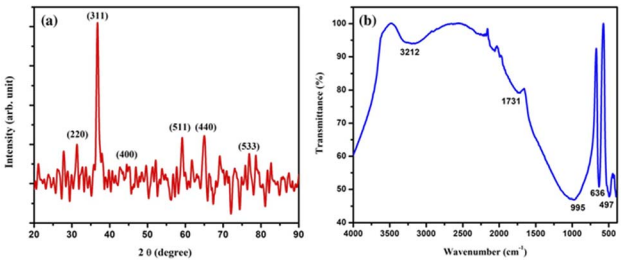

Fig. 2 The (a) powder XRD pattern, and (b) FT-IR spectrum of $NiCo_2O_4$ nanomaterial.

hydroxide solution (5 M) was prepared in double-distilled water and then added drop by drop to the resulting solution by stirring until the pH of the resulting solution became 10.0. Then, the blue precipitate was formed, and the whole solution gradually turned grey. Thereafter, it was left for 2 h with continuous stirring. After that, the solution was made alkali-free (pH 6.0–7.0) by washing again and again with distilled water, and then the precipitate was filtered and dried in a hot air oven overnight at 80 °C. Finally, the solid material was ground and calcined at 400 °C for 3 h. The obtained black material was analyzed by different characterization techniques (Scheme 2).

The powder X-ray diffraction (XRD) analysis of nano-$NiCo_2O_4$ was carried out using a Rigaku Ultima IV X-ray diffractometer with Cu Kα radiation ($\lambda = 1.540806$ Å), operating at 40 kV and 40 mA, with a step size of 0.02° and a scanning rate of 0.24° min^{-1}. The FESEM was performed using a JSM-7610FPlus Schottky field emission scanning electron microscope with an energy of 5 keV. The High-resolution transmission electron microscopy (HR-TEM) of nano-$NiCo_2O_4$ was performed using a JEOL 4000 EX/II operating at 400 kV (point-to-point resolution of 0.165 nm) and a JEOL 2010 FEG operating at 200 kV (information limit of 0.11 nm). Fourier-transform infrared (FT-IR) spectroscopy was conducted using a Thermo Scientific Nicolet Summit X spectrometer equipped with a diamond ATR crystal, DTGS–KBr detector, and a KBr beamsplitter.

3 Results and discussion

3.1 Characterization of $NiCo_2O_4$

To study the structural properties and to identify the phase of samples, powder X-ray diffraction (PXRD) measurements were carried out using D8 Advance Bruker with Cu K-alpha source. All diffraction patterns were recorded with 2θ ranging from 10° to 70° at a low scan rate of 0.5° per minute. PXRD was performed to analyze the chemical structure of $NiCo_2O_4$ (Fig. 2a). Well-defined diffraction peaks are observed at $2\theta = 31.29°$, 36.6°, 44.4°, 59.1°, 65.1°, and 76.8° which correspond to the crystalline planes of (220), (311), (400), (511), (440), and (533), respectively. All diffraction peaks correspond to the cubic spinel phase of $NiCo_2O_4$ (JCPDS Card No. 20–0781).[47] The particle size of crystals in the form of powder can be determined by the Scherrer equation, $\left(D = \frac{0.9\lambda}{\beta \cos \theta}\right)$, where $\lambda = 1.54$ Å and β is the FWHM and θ is the Bragg's diffraction angle, by considering the FWHM of the (311) diffraction plane. The crystallite size, as calculated from XRD, is 121.69 nm. The FTIR spectrum (Fig. 2b) shows broad O–H stretching at 3212 cm^{-1} due to surface hydroxyls and two characteristic peaks at 487 and 630 cm^{-1} related to Co–O and Ni–O vibrations, respectively. Bands at 1731 and 995 cm^{-1} may arise due to carboxylate groups.[47]

The morphology of the so-prepared material was analyzed using the field emission scanning electron microscope (FESEM) images (Fig. 3a) and High-Resolution Transmission Electron Microscopy (HRTEM) images (Fig. 4a). It is observed that the morphology is composed of roughly spherical-shaped granules. The mean size of the nanoparticles is calculated to be 0.251 µm using ImageJ software, based on the measurements of 200 individual granules. Further, for the elemental composition of nanomaterials, the EDS spectrum analysis of fabricated $NiCo_2O_4$ was carried out (Fig. 3b), which reveals four prominent peaks corresponding to Ni, Co, and O. During the SEM imaging, a thin Pt coating was applied to improve surface conductivity and image resolution, due to which the EDX spectrum inevitably shows a Pt signal originating from this conductive coating rather than from the sample itself. Thus, with no detectable impurity signals, it confirms the elemental purity of the material.

The granular nanoparticles are more prominently visible in the HRTEM images, with a granular size ranging from 1.5 to 3 nm and a mean size of 2.25 nm. The surface and porosity of the as-prepared material, $NiCo_2O_4$, were thoroughly characterized using nitrogen adsorption–desorption measurements based on the Brunauer–Emmett–Teller (BET) theory. The obtained isotherm exhibited a characteristic Type IV profile with a distinct hysteresis loop, according to the IUPAC classification, indicative of a mesoporous material (Fig. 4b).

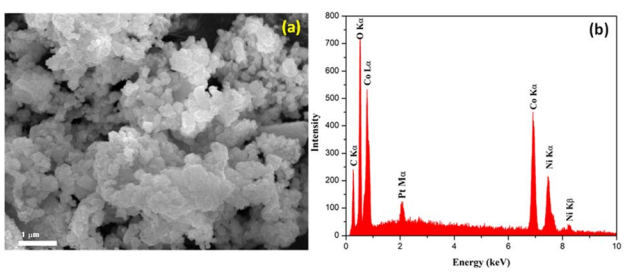

Fig. 3 The (a) FESEM image, and (b) EDX spectra of $NiCo_2O_4$ nanomaterial.

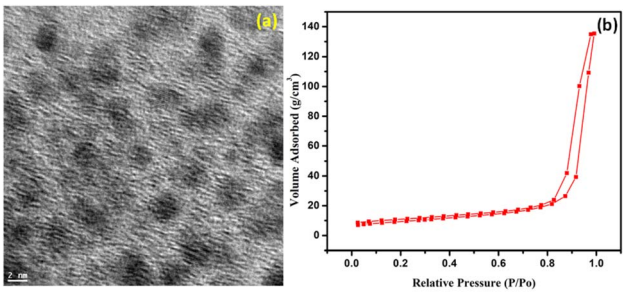

Fig. 4 The (a) TEM image, and (b) nitrogen adsorption and desorption isotherms of $NiCo_2O_4$.

The BET surface area of the $NiCo_2O_4$ sample was determined to be 33.81 $m^2\ g^{-1}$, reflecting a moderately developed porous network. Furthermore, analysis using the Barrett–Joyner–Halenda (BJH) method revealed a cumulative pore volume of 0.2102 $cm^3\ g^{-1}$ and an average pore diameter of 23.49 nm, reinforcing the mesoporous nature of the material.[48] Although the BET surface area (33.81 $m^2\ g^{-1}$) lies within a moderate range for $NiCo_2O_4$ nanoparticles, the presence of well-developed mesoporosity (23.49 nm) and a relatively high pore volume (0.2102 $cm^3\ g^{-1}$) provides efficient mass transport and exposes a greater fraction of redox-active Ni and Co sites. This could help significantly with the catalytic activity. Moreover, the presence of large mesopores facilitates the rapid removal of evolved H_2 gas.

3.2 $NiCo_2O_4$-catalyzed dehydrogenative esterification of primary alcohol

Next, the catalytic activity of well-characterized $NiCo_2O_4$ NPs was examined in the direct conversion of primary alcohols into esters. We started by using benzyl alcohol as a model substrate and optimizing the reaction conditions. The findings are shown in Table 1. Initially, a mixture of benzyl alcohol (1.0 mmol), methyl alcohol (2.0 mL), $NiCo_2O_4$ (50 mg), and KOH (3.0 equivalents) was stirred at room temperature for 12 hours (entry 1, Table 1), with no reaction observed.

However, increasing the temperature gradually improved the yield of the model reaction, reaching an excellent 95% yield of methyl benzoate after workup (entry 2, Table 1). The presence of methyl benzoate was indicated by the distinctive fruity or sweet aroma of the reaction mixture, confirmed further through ^1H NMR spectroscopy. To assess the effect of the base, the reaction was performed without KOH. Only benzyl alcohol was recovered even after heating at 120 °C for 12 hours (entry 3, Table 1), confirming the critical role of the base. Next, we optimized the amounts of catalyst and base (entries 4–7, Table 1). It was found that 30 mg of catalyst (entry 5, Table 1) and 2.0 equivalents of KOH (entry 7, Table 1) were sufficient to convert benzyl alcohol into methyl benzoate with an excellent yield (entry 6, Table 1). We then compared the catalytic activity of $NiCo_2O_4$ with other cobaltite materials. Reactions with Co_3O_4, $CuCo_2O_4$, and $ZnCo_2O_4$ produced trace amounts, 60%, and 72% esters, respectively (entries 8–10, Table 1). Replacing KOH with NaOH resulted in a lower ester yield (entry 11, Table 1). When the model reaction was performed under microwave irradiation (power 80 W) instead of conventional heating, 82% of ester was formed within 5 minutes at 120 °C (entry 12, Table 1), and within 10 minutes, benzyl alcohol was fully converted into methyl benzoate with a 92% isolated yield (entry 13, Table 1). Microwave-assisted synthesis is now a well-established methodology in modern organo-catalytic chemistry. The Microwave (MW) irradiation markedly accelerates reaction kinetics and enhances product formation efficiency due to its unique ability to transfer optimal heat by selective volumetric dielectric heating, along with other advantages such as improved selectivity, higher product yields, safety, energy efficiency, and environmental friendliness, aligning with green chemistry principles.[49] However, reducing the temperature under microwave-irradiation conditions decreased the yield. Therefore, microwave irradiation (120 °C, 80 W power) of a mixture of benzyl alcohol (1.0 mmol), $NiCo_2O_4$ (30 mg), KOH (2.0 equiv.), and methyl alcohol (2 mL) for 10 min. was established as the optimized reaction condition (entry 13, Table 1).

Next, using optimized reaction conditions, we investigated the esterification of a series of structurally diverse benzylic

Table 1 Optimization of reaction conditions for the conversion of benzyl alcohol to methyl benzoate[a]

Entry	Catalyst/Amount (in mg)	Base (equiv.)	Temp (°C)	Time	Yield (%)
1	$NiCo_2O_4$ (50)	KOH (3.0)	R.T.	12 h	—
2	$NiCo_2O_4$ (50)	KOH (3.0)	120	10 h	95
3	$NiCo_2O_4$ (50)	—	120	12 h	—
4	$NiCo_2O_4$ (40)	KOH (3.0)	120	12 h	93
5	$NiCo_2O_4$ (30)	KOH (3.0)	120	12 h	91
6	$NiCo_2O_4$ (20)	KOH (3.0)	120	12 h	80
7	$NiCo_2O_4$ (30)	KOH (2.0)	120	12 h	91
8	Co_3O_4 (30)	KOH (2.0)	120	12 h	20
9	$CuCo_2O_4$ (30)	KOH (2.0)	120	12 h	60
10	$ZnCo_2O_4$ (30)	KOH (2.0)	120	12 h	72
11	$NiCo_2O_4$ (20)	NaOH (2.0)	120	12 h	50
12	$NiCo_2O_4$ (30)	KOH (2.0)	MW/120	5 min	82[b]
13	$NiCo_2O_4$ (30)	KOH (2.0)	MW/120	10 min	92[b]

[a] Reaction conditions: benzyl alcohol (1.0 mmol), MeOH (2.0 mL), catalyst, base. [b] MW (80 Watts). Isolated yield after workup.

alcohols. The results are presented in Table 2. Different benzyl and cinnamyl alcohol derivatives with –Cl, –NO_2, –OMe, and –Me functional groups at *o*/*m*/*p*-positions of the aromatic ring smoothly participated in the $NiCo_2O_4$-catalyzed dehydrogenative esterification reactions. Further, methyl, ethyl, and *n*-propyl derivatives of aryl and cinnamyl esters were synthesized by using the corresponding alcohols as solvents. To further expand the substrate scope, the protocol was applied to both heterocyclic and aliphatic alcohols. These were successfully transformed into the corresponding esters (Table 2; **2p**, **2q**, and **2r**), although the reactions proceeded with only moderate isolated yields (50–65%).

All the $NiCo_2O_4$ catalyzed dehydrogenative esterification reactions are very clean, fast (10 min), high-yielding (50–92%), and require no oxidant, additives, or ligands. The exceptional catalytic performance of the material can be attributed to its textural and structural features. The ultrafine granular nanoparticles observed in the HRTEM images (1.5–3 nm, mean size: 2.25 nm) expose a high population of surface atoms, thereby increasing the number of accessible Ni and Co redox sites

Table 2 Scope of $NiCo_2O_4$-catalyzed oxidation of benzyl alcohols to the corresponding ester[a]

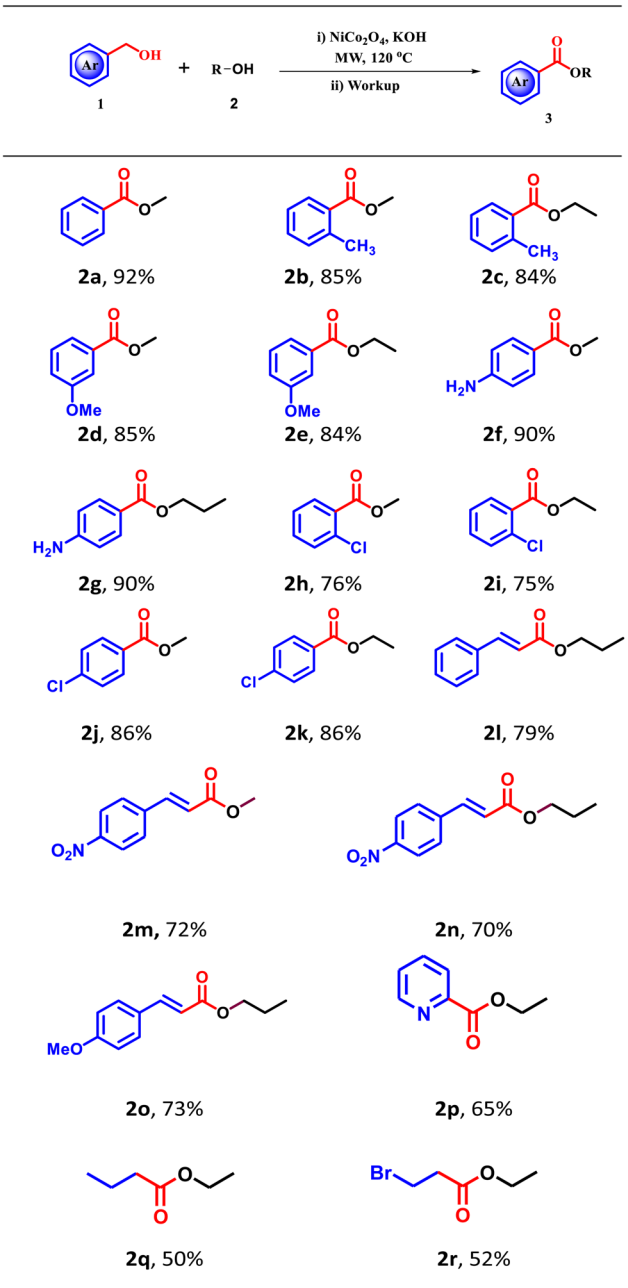

[a] Reaction conditions: aryl alcohol (1.0 mmol), catalyst (30 mg), base (2.0 equiv.), alcohol (2 mL), MW (80 Watts). The yields refer to the isolated pure products.

Table 3 A comparative study of the present method with the previously reported methods

Entry	Catalyst	Conditions	Yield (%)	Ref.
1	Pyridine-based PNNH–Ru pincer complexes	KO^{t}Bu, 45 °C/40–144 h/Argon flow	<1–97%	33
2	[(^{iPr}PPPN^{Me}Py^{Me})CoCl]OTf	KO^{t}Bu/125–140 °C/24 h	28–93%	34
3	[$RhCl_3$(tpy)]	$NaHCO_3$/90 °C/12–48 h	54–96%	35*a*
4	Mn(^{Ph}PNN)$(CO)_2$Br	^{t}BuOK/120 °C/24 h	71–95%	35*b*
5	Dicationic Cp*Ir complex	Cs_2CO_3/120 °C/24 h, argon gas	64–96%	35*c*
6	Pt/SnO_2	Neat, 180 °C/36 h N_2 atmosphere	53–91%	36
7	$NiCo_2O_4$	KOH/80 W, 120 °C/10 min	50–92%	Present work

required for efficient catalysis. Also, the mesoporosity of the material, as confirmed by the BET analysis, enables rapid diffusion of reactants and products throughout the catalytic framework.

Moreover, the catalyst $NiCo_2O_4$ is robust and easily fabricated from abundantly available and inexpensive starting materials, making this protocol a more attractive alternative to existing protocols. A comparative study of the present method with the previously reported methods of dehydrogenative oxidation has been provided in Table 3.

The comparison table clearly shows that most catalytic systems are moisture-sensitive and expensive, requiring elevated reaction temperatures and long reaction times (12–144 h). Additionally, these methods require strong bases and inert conditions to achieve good yields. However, the present $NiCo_2O_4$ catalyzed esterification provides a high yield in comparatively less time (10 min). Additionally, the catalyst is reusable, highlighting its practical advantage over previously reported methods.

3.3 $NiCo_2O_4$-catalyzed dehydrogenative amidation of primary alcohol

Motivated by the excellent catalytic activity of $NiCo_2O_4$ NPs towards dehydrogenative esterification of primary alcohols, we next explored the catalytic activity towards the dehydrogenative amidation reaction of primary alcohols. When a mixture of benzyl alcohol (1.0 mmol), $NiCo_2O_4$ (30 mg), KOH (2.0 equiv.), and benzyl amine (1.0 mmol) was irradiated with MW radiation at 80 W power, 120 °C, 10 min, a good yield of *n*-phenylbenzamide (80%) was obtained. Further, the scope of the protocol was extended to the amidation of benzyl alcohols with different aliphatic and aromatic amines. The corresponding results are summarized in Table 4.

Heterogeneous catalysts often face challenges related to metal leaching, which can affect their stability and reusability. To examine the heterogeneity of $NiCo_2O_4$, a hot filtration test was performed. Oxidation of benzyl alcohol (1 mmol) to methyl benzoate was chosen as the model reaction. After 2 minutes of reaction (32% conversion), the catalyst was rapidly separated from the reaction mixture by ultracentrifugation under hot conditions. The resulting clear filtrate was then stirred under identical reaction conditions for an additional 8 minutes, and the progress of the reaction was monitored at an interval of 2 minutes. No further conversion was observed after catalyst removal, indicating the absence of active catalytic species in the solution and highlighting the robustness and reusability of the $NiCo_2O_4$ nanoparticles under the applied conditions. The error bars shown in Fig. 5a correspond to the standard deviation

Table 4 Scope of $NiCo_2O_4$-catalyzed oxidation of benzyl alcohol to corresponding amides[a]

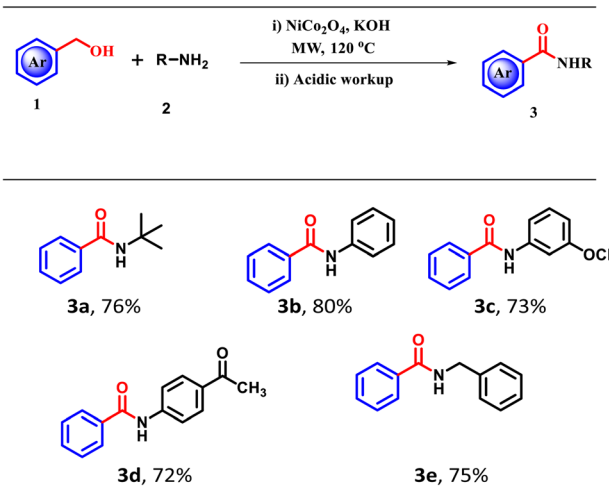

[a] Reaction conditions: benzyl alcohol (1.0 mmol), catalyst (30 mg), base (2.0 equiv.), aryl/alkyl amine (1.0 mmol), MW (80 Watts). The yields refer to the isolated pure products.

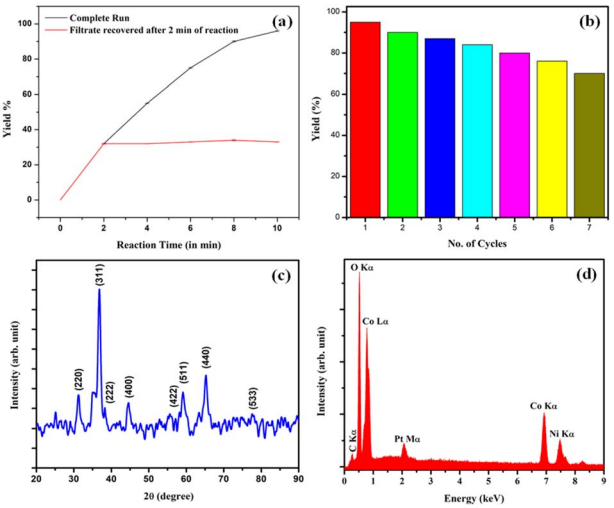

Fig. 5 (a) Leaching study by hot filtration method (with error bars), (b) reusability test of the $NiCo_2O_4$ for the synthesis of methyl benzoate as the model reaction, (c) powder XRD pattern of recycled $NiCo_2O_4$, and (d) EDX of the reused catalyst.

derived from three independently repeated hot filtration experiments performed under identical reaction conditions. The consistently small size of error bars reflects high experimental reproducibility.

Next, we have investigated the stability and reusability of nano-$NiCo_2O_4$, choosing the same model reaction. The results are presented in Fig. 5a. After each run, the catalyst was recovered by centrifugation, washed with methanol, dried in an oven at 80 °C for 6 h, and reused for subsequent runs. It was observed that the catalyst remained stable and active up to eight runs. However, after the fifth cycle onwards, a considerable loss in the yield of the product was observed. This could be attributed to the physical loss of the catalyst during the filtration and washing steps involved in the reusability test (Fig. 5b). The PXRD analysis and EDS spectra of the reused catalyst are given in Fig. 5c and d, respectively. A comparison between the EDX spectra of the fresh and reused catalysts shows no emergence of additional peaks, indicating that the elemental composition of $NiCo_2O_4$ remains intact. Also, the PXRD pattern of the reused catalyst is similar to that of the fresh catalyst. Thus, the material retains its stability even after multiple catalytic cycles.

In addition to the physical loss of catalyst during repetitive recycling steps, the decline in catalytic activity observed after the fifth cycle may also be attributed to subtle nanoparticle agglomeration and the gradual formation of surface-bound oxidised species. These changes can result in limited access to active sites, thereby reducing the overall efficacy of the catalyst after recycling.

We have performed the reaction in an inert nitrogen atmosphere. It is observed that the reaction takes place smoothly even under a nitrogen atmosphere. To check the oxidation state of Ni and Co, CV (cyclic voltammetry) of fresh $NiCo_2O_4$, recycled $NiCo_2O_4$ obtained after reaction performed under air, and recycled $NiCo_2O_4$ obtained after reaction performed under inert

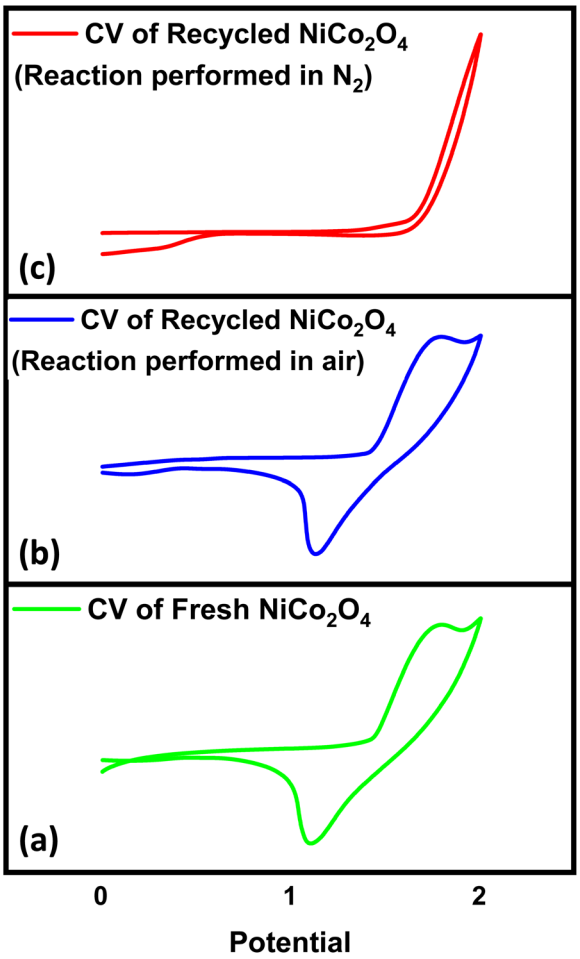

Fig. 6 The CV pattern of (a) fresh $NiCo_2O_4$ and recovered $NiCo_2O_4$ after reaction performed (b) in air, and (c) in N_2 atmosphere.

N_2 atmosphere was performed (Fig. 6). It is observed that the CV patterns of fresh $NiCo_2O_4$ and recycled $NiCo_2O_4$ obtained from the reaction performed under air are similar, which indicates the reoxidation of Ni (0) to Ni(II) by aerial oxidation. However, the CV pattern of recycled $NiCo_2O_4$, in which the reaction is performed under an inert nitrogen atmosphere, is different from the CV pattern of fresh $NiCo_2O_4$. Here, the CV pattern indicates the formation of Ni (0). This validates the requirement of molecular oxygen from air to regenerate the catalyst and continue the catalytic cycle.

To elucidate the reaction mechanism, a series of experiments was conducted (Scheme 3). 1 mmol of benzyl alcohol was taken in the presence of $NiCo_2O_4$ (30 mg), KOH (2 equiv.), MeOH (2 mL) under microwave conditions for 10 min resulted in the formation of methyl benzoate in 92% yield (eqn (i). Scheme 3). In contrast, replacing $NiCo_2O_4$ with Co_3O_4 under identical conditions resulted in significantly lower yields of benzaldehyde (10%) and methyl benzoate (5%), highlighting the critical role of Ni in promoting dehydrogenative oxidation (eqn (ii). Scheme 3).

Further, in a closed vessel, 1 mmol of nitrophenol was added to 1 mmol of benzyl alcohol under similar reaction conditions,

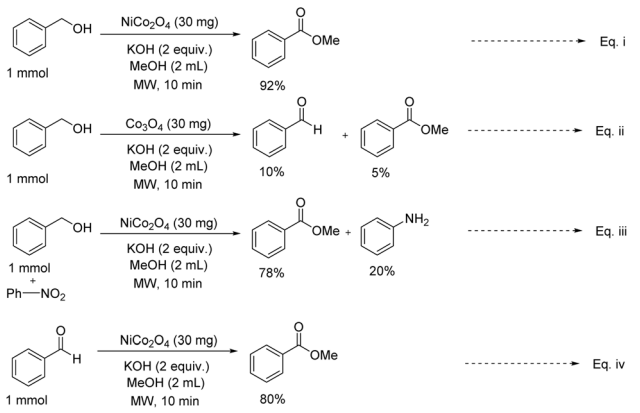

Scheme 3 Mechanistic study for the dehydrogenative oxidation of alcohol to ester.

which resulted in the formation of methyl benzoate and aniline (eqn (iii). Scheme 3). The formation of reduction products from *p*-nitrophenol strongly suggests *in situ* hydrogen evolution during the transformation. Moreover, the conversion of benzaldehyde (1 mmol) to methyl benzoate under identical conditions supports that benzaldehyde might be formed as an intermediate during the dehydrogenative oxidation of alcohols (eqn (iv). Scheme 3). Based on the above control experiments and previously reported mechanism of dehydrogenative esterification,[35b] we have presented a plausible mechanistic catalytic cycle for $NiCo_2O_4$-catalyzed dehydrogenation of primary alcohol, in Fig. 7. Initially, the primary alcohol undergoes coordination with the Ni-center of the $NiCo_2O_4$ catalyst, facilitating the activation of the O–H bond. This results in the formation of a surface-bound alkoxy species on $NiCo_2O_4$, accompanied by the release of a proton, which subsequently reacts with hydroxide to generate water.

The alkoxy species then undergoes β-hydride elimination, affording the corresponding aldehyde along with the evolution of molecular hydrogen (H_2). Subsequently, MeOH attacks the *in situ*-generated aldehyde, leading to the formation of a hemiacetal-type intermediate. Deprotonation of this intermediate by KOH yields a Ni-coordinated intermediate. Upon completion of the reaction and subsequent workup, these intermediates yield the corresponding ester product, accompanied by the evolution of additional H_2 gas. A similar mechanistic approach will be followed in the case of amidation as well. Instead of MeOH, aniline acts as the nucleophile and attacks the generated aldehyde.

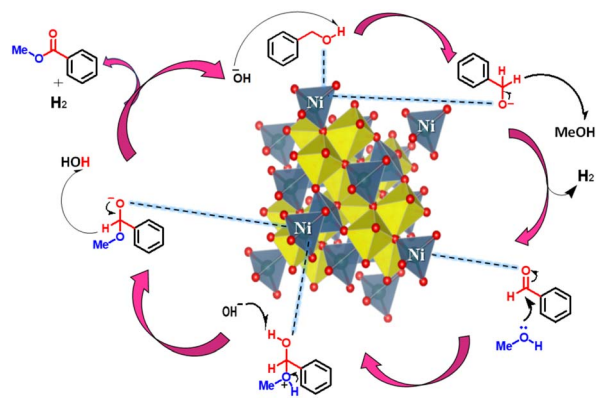

Fig. 7 Plausible mechanism of $NiCo_2O_4$-catalyzed dehydrogenative esterification of benzyl alcohol.

4 Conclusions

In summary, we synthesized $NiCo_2O_4$ nanomaterials *via* the co-precipitation method, and the structural properties of the mesoporous polycrystalline cubic spinel phase $NiCo_2O_4$ nanomaterials were characterized through powder XRD, FESEM, EDAX, TEM, and BET analyses. The crystallite size of the uniform-sized spherical NPs was calculated to be 121.69 nm from XRD. The FESEM shows the formation of roughly spherical granules with a mean size of the NPs to be 2.23 μm. The granular nanoparticles are more prominently visible in the HRTEM images, with a granular size ranging from 1.5 to 3 nm and a mean size of 2.25 nm. Further, the EDS spectrum confirms the elemental purity of the material by showing prominent peaks of Ni, Co, and O in the spectrum. Moreover, the BET surface area of the $NiCo_2O_4$ sample was determined to be 33.81 $m^2\ g^{-1}$, suggesting a moderately developed porous network. Also, the analysis using the Barrett–Joyner–Halenda (BJH) method reveals a cumulative pore volume of 0.2102 $cm^3\ g^{-1}$ and an average pore diameter of 23.49 nm, reaffirming the mesoporous nature of the material. Further, an efficient catalytic performance of these nanomaterials was evaluated in a one-pot dehydrogenative esterification and amidation of primary alcohols under microwave irradiation. Notably, these transformations occurred under oxidant- and solvent-free conditions, releasing hydrogen gas as the only by-product. This method achieved good to excellent product yields of esters (50–92%) and amides (72–80%) and showed broad tolerance toward various functional groups. A plausible mechanism of dehydrogenative direct oxidation of alcohol to ester has been provided, and the mechanism was supported by control experiments. Moreover, cyclic voltametric studies of fresh and recycled $NiCo_2O_4$ prove the role of aerial oxygen in regenerating the catalyst and sustaining the catalytic cycle. This study highlights the potential of $NiCo_2O_4$ as a robust, low-cost, eco-friendly catalyst for green and sustainable synthesis of value-added organic compounds.

Author contributions

Kumari Anchal: material preparation, dehydrogenative esterification and amidation of alcohols, NMR analysis, *etc.* Keya Roy: amide synthesis and performed NMR analysis. Laksmikanta Adak: manuscript preparation supervision. Subhash Banerjee: supervision, concept, final draft preparation, *etc.*

Conflicts of interest

There are no conflicts to declare.

Data availability

The data supporting this article have been included as part of the supplementary information (SI). Supplementary information: copies of ^{1}H NMR and ^{13}C NMR spectra of all the products listed in Tables 2 and 3 are available in the supporting information. See DOI: https://doi.org/10.1039/d5ra07245j.

Acknowledgements

We are pleased to acknowledge the ANRF PAIR project (FN-ANRF/PAIR/2025/000003/PAIR-B) funded by the Department of Science & Technology (DST), Government of India, and ANRF (ANRF, erstwhile SERB, DST, Government of India) and DSTBT, Govt. of West Bengal for financial support. We are also grateful to Prof. Ashish Kumar Singh and Pappu Shriwas for their valuable support in carrying out the cyclic voltammetry (CV) experiments.

References

1 S. Ortega-Requena, C. Montiel, F. Máximo, M. Gómez, M. D. Murcia and J. Bastida, *Materials*, 2024, **17**, 268.
2 M. Tian, R. L. McCormick, J. Luecke, E. de Jong, J. C. van der Waal, G. P. van Klink and M. D. Boot, *Fuel*, 2017, **202**, 414–425.
3 J. Otera and J. Nishikido, *Esterification: Methods, Reactions, and Applications*, John Wiley & Sons, USA, 2019, pp. 293–320.
4 R. J. Ouellette and J. D. Rawn, *Carboxylic Acids in Organic Chemistry*, Elsevier, 2014, pp. 659–698.
5 K. M. Kulkarni, S. A. Jadhav, P. B. Patil, V. R. Dhole and S. S. Patil, *Pharma Chem.*, 2016, **8**, 1–5.
6 R. C. Batterman and C. K. Himmelsbach, *J. Am. Med. Assoc.*, 1943, **122**, 222–226.
7 S. Trifilio, L. Gordon, H. Rubin, N. Grosshans and J. Mehta, *Support. Care Cancer*, 2021, **29**, 3643–3648.
8 G. F. Valle, R. C. Biesterfeld and J. F. Taintor, *J. Endod.*, 1979, **5**, 201–207.
9 L. Wang, C. Hu, X. Yang, Y. Fu and Z. Du, *Eur. J. Org Chem.*, 2024, **27**, e202400032.
10 J. Yin, Y. Zhao, Q. He, A. Hai and Y. Peng, *et.al.*, *Bioorg. Med. Chem. Lett.*, 2022, **60**, 128587.
11 G. C. de Freiras, R. T. Pozzobon, D. S. Blaya and C. H. Moreira, *Anesth. Prog.*, 2015, **62**, 46–50.
12 H. C. Kimko, J. T. Cross and D. R. Abernethy, *Clin. Pharmacokinet.*, 1999, **37**, 457–470.
13 A. C. de Castro, F. A. Nascimento, Á. Beltran-Corbellini, R. Toledano, I. Garcia-Morales, A. Gil-Nagel and Á. Aledo-Serrano, *Seizure-Eur. J. Epilep.*, 2023, **107**, 121–131.
14 (*a*) A. Bar-Or, H. Wiendl, B. Miller, M. Benamor, P. Truffinet, M. Church and F. Menguy-Vacheron, *Neurol. Neuroimmunol. Neuroinflamm.*, 2015, **2**, e70; (*b*) Y. Zheng, C. Huang, Y. Li, Y. Yang and R. Xu, *ChemCatChem*, 2024, **16**, e202300976.
15 (*a*) J. Otera and J. Nishikido, Esterification: Methods, Reactions, and Applications, *International Journal of Organic Chemistry*, Wiley-VCH, Weinheim, 2010; (*b*) L. E. Barstow and V. J. Hruby, *J. Org. Chem.*, 1971, **36**, 1305–1306; (*c*) F. A. Carey and R. G. Sundbery, in *Advanced Organic Chemistry, Part B: Reactions and Synthesis*, Springer, New York, 5th edn, 2007; (*d*) K. Ekoue-Kovi and C. Wolf, *Chem.–Eur. J.*, 2008, **14**, 6302–6315; (*e*) S. Tang, J. Yuan, C. Liu and A. Lei, *Dalton Trans.*, 2014, **43**, 13460–13470.
16 S. Gowrisankar, H. Neumann and M. Beller, *Angew. Chem., Int. Ed.*, 2011, **50**, 5139–5143.
17 X. F. Bai, F. Ye, L. S. Zheng, G. Q. Lai, C. G. Xia and L. W. Xu, *ChemComm.*, 2012, **48**, 8592–8594.
18 C. Liu, S. Tang and A. Lei, *ChemComm.*, 2013, **49**, 1324–1326.
19 C. Liu, J. Wang, L. Meng, Y. Deng, Y. Li and A. Lei, *Angew. Chem., Int. Ed.*, 2011, **50**, 5144–5148.
20 P. van Bonn, D. Dreßler, F. Weitenhagen and C. Bolm, *ACS Sustain. Chem. Eng.*, 2022, **10**, 1361–1366.
21 J. Zhang, G. Leitus, Y. Ben-David and D. Milstein, *J. Am. Chem. Soc.*, 2005, **127**, 10840–10841.
22 M. Nielsen, H. Junge, A. Kammer and M. Beller, *Angew. Chem., Int. Ed.*, 2012, **51**, 1–4.
23 N. A. Owston, A. J. Parker and J. M. Williams, *ChemComm.*, 2008, **5**, 624–625.
24 J. H. Dam, G. Osztrovszky, L. U. Nordstrøm and R. Madsen, *Chem.–Eur. J.*, 2010, **16**, 6820–6827.
25 L. U. Nordstrøm, H. Vogt and R. Madsen, *J. Am. Chem. Soc.*, 2008, **130**, 17672–17673.
26 C. Chen, Y. Zhang and S. H. Hong, *J. Org. Chem.*, 2011, **76**, 10005–10010.
27 R. L. Oliveira, P. K. Kiyohara and L. M. Rossi, *Green Chem.*, 2009, **11**, 1366–1370.
28 H. Miyamura, T. Yasukawa and S. Kobayashi, *Green Chem.*, 2010, **12**, 776–778.
29 F. Z. Su, J. Ni, H. Sun, Y. Cao, H. Y. He and K. N. Fan, *Chem.–Eur. J.*, 2008, **14**, 7131–7135.
30 C. Milone, R. Ingoglia, G. Neri, A. Pistone and S. Galvagno, *Appl. Catal., A*, 2001, **211**, 251–257.
31 K. Kaizuka, H. Miyamura and S. Kobayashi, *J. Am. Chem. Soc.*, 2010, **132**, 15096–15098.
32 N. Yamamoto, Y. Obora and Y. Ishii, *J. Org. Chem.*, 2011, **76**, 2937–2941.
33 (*a*) E. Fogler, J. A. Garg, P. Hu, G. Leitus, L. J. Shimon and D. Milstein, *Chem.–Eur. J.*, 2014, **20**, 15727–15731; (*b*) C. Gunanathan and D. Milstein, *Chem. Rev.*, 2014, **114**, 12024–12087.
34 K. Paudel, B. Pandey, S. Xu, D. K. Taylor, D. L. Tyer, C. L. Torres, *et al.*, *Org. Lett.*, 2018, **20**, 4478–4481.
35 (*a*) J. Cheng, M. Zhu, C. Wang, J. Li, X. Jiang, Y. Wei, W. Tang, D. Xue and J. Xiao, *Chem. Sci.*, 2016, **7**, 4428–4434; (*b*) U. K. Das, Y. B. David, G. Leitus, Y. D. Posner and D. Milstein, *ACS Catal.*, 2019, **9**(1), 479–484; (*c*) M. Onoda and K. Fujita, *ChemistrySelect*, 2022, **7**(30), e202201135.
36 S. K. Moromi, S. H. Siddiki, M. A. Ali, K. Kon and K. Shimizu, *Catal. Sci. Technol.*, 2014, **4**, 3631–3635.
37 C. Gunanathan, Y. Ben-David and D. Milstein, *Science*, 2007, **317**, 790–792.
38 S. C. Ghosh, S. Muthaiah, Y. Zhang, X. Xu and S. H. Hong, *Adv. Synth. Catal.*, 2009, **351**, 2643–2649.
39 S. C. Ghosh, J. E. Jee, C. Chen, J. Zhang and S. H. Hong, *J. Org. Chem.*, 2010, **75**, 3002–3006.

40 T. Zweifel, J. V. Naubron and H. Grützmacher, *Angew. Chem.*, 2009, **121**, 567–571.
41 E. M. Lane, K. B. Uttley, N. Hazari and W. Bernskoetter, *Organomet. Chem.*, 2017, **36**, 2020–2025.
42 A. Kumar, N. A. Espinosa-Jalapa, G. Leitus, Y. Diskin-Posner, L. Avram and D. Milstein, *Angew. Chem., Int. Ed.*, 2017, **56**, 14992–14996.
43 K. I. Shimizu, K. Ohshima and A. Satsuma, *Chem.–Eur. J.*, 2009, **15**, 9977–9980.
44 (*a*) S. Gu, Z. Lou, X. Ma and G. Shen, *ChemElectroChem*, 2015, **2**, 1042–1047; (*b*) A. Serov, N. I. Andersen, A. J. Roy, I. Matanovic, K. Artyushkova and P. J. Atanassov, *J. Electrochem. Soc.*, 2015, **162**, 449–454; (*c*) S. Anke, T. Falk, G. Bendt, I. Sinev, M. Havecker, H. Antoni, I. Zegkinoglou, *et al.*, *ACS Catal.*, 2020, **382**, 57–68.
45 (*a*) C. Yuan, J. Li, L. Hou, X. Zhang, L. Shen and X. W. D. Lou, *Adv. Funct. Mater.*, 2012, **22**, 4592–4597; (*b*) H. Wang, Q. Gao and L. Jiang, *Small*, 2011, **7**, 2454–2459; (*c*) Q. Wang, B. Liu, X. Wang, S. Ran, L. Wang, D. Chen and G. J. Han, *J. Mater. Chem.*, 2012, **22**, 21647–21653; (*d*) T. Y. Wei, C. H. Chen, H. C. Chien, S. Y. Lu and C. C. Hu, *Adv. Mater.*, 2010, **22**, 347–351; (*e*) R. Zou, K. Xu, T. Wang, G. He, Q. Liu, X. Liu, Z. Zhang and J. Hu, *J. Mater. Chem. A*, 2013, **1**, 8560–8566; (*f*) H. Jiang, J. Ma and C. Li, *Chem. Commun.*, 2012, **48**, 4465–4467; (*g*) Z. Zhang, Y. Wang, Z. An, M. Pan, M. Zhao, K. Song and X. Hu, *Mater. Today Commun.*, 2024, **38**, 108243.
46 (*a*) S. Banerjee and A. Saha, *New J. Chem.*, 2013, **37**, 4170–4175; (*b*) S. Banerjee, S. Payra, A. Saha and G. Sereda, *Tetrahedron Lett.*, 2014, **55**, 5515–5520; (*c*) A. Saha, S. Payra and S. Banerjee, *Green Chem.*, 2015, **17**, 2859–2866; (*d*) S. Payra, A. Saha and S. Banerjee, *RSC Adv.*, 2016, **6**, 12402–12407; (*e*) S. Payra, A. Saha, S. Guchhait and S. Banerjee, *RSC Adv.*, 2016, **6**, 33462–33467; (*f*) S. Payra, A. Saha and S. Banerjee, *RSC Adv.*, 2016, **6**, 52495–52499; (*g*) S. Payra, A. Saha and S. Banerjee, *ChemistrySelect*, 2018, **3**, 7535–7540; (*h*) A. Saha, S. Payra, B. Selvaratnam, S. Bhattacharya, S. Pal, R. T. Koodali and S. Banerjee, *ACS Sustain. Chem. Eng.*, 2018, **6**, 11345–11352; (*i*) A. R. Patel, A. Asatkar, G. Patel and S. Banerjee, *ChemistrySelect*, 2019, **4**, 5577–5584; (*j*) A. R. Patel, G. Patel and S. Banerjee, *ACS Omega*, 2019, **4**, 22445–22455; (*k*) A. R. Patel, G. Patel, G. Maity, S. P. Patel, S. Bhattacharya, A. Putta and S. Banerjee, *ACS Omega*, 2020, **5**, 30416–30424; (*l*) G. Patel, A. R. Patel, T. L. Lambat, S. H. Mahmood and S. Banerjee, *FlatChem*, 2020, **21**, 100163; (*m*) G. Patel, A. R. Patel, T. L. Lambat and S. Banerjee, *Curr. Res. Green Sustainable Chem.*, 2021, **4**, 100149; (*n*) G. Patel, A. R. Patel, G. Maity, S. Das, S. P. Patel and S. Banerjee, *Curr. Res. Green Sustainable Chem.*, 2022, **5**, 100258; (*o*) A. R. Patel, G. Maity, T. K. Pati, L. Adak, C. L. Cioffi and S. Banerjee, *Front. Chem.*, 2024, **12**, 1496234; (*p*) K. Anchal, A. R. Patel and S. Banerjee, *Synlett*, 2024, **35**(20), 2409–2416; (*q*) S. Sharma and S. Banerjee, *ChemistrySelect*, 2025, **10**(17), e202500512.
47 (*a*) N. E. A. El-Gamel, S. S. Medany and M. A. Hefnawy, *Sci. Rep.*, 2025, **15**, 14402; (*b*) T. L. Simonenko, N. P. Simonenko, A. S. Mokrushin, P. Y. Gorobtsov, A. A. Lizunova, O. Y. Grafov, E. P. Simonenko and N. T. Kuznetsov, *Chemosensors*, 2023, **11**, 138; (*c*) S. Hassanpoor and F. Aghely, *RSC Adv.*, 2020, **10**, 35235–35244.
48 V. Shanmugavalli, R. D. Kumar, A. J. Kumar, R. Kavitha, C. Brundha, V. Sampath and M. Lee, *J. Mater. Sci.: Mater. Electron.*, 2023, **34**, 849.
49 (*a*) K. Martina, G. Cravotto and R. S. Varma, *J. Org. Chem.*, 2021, **86**(20), 13857–13872; (*b*) M. Caporaso, G. Cravotto, S. Georgakopoulos, G. Heropoulos, K. Martina and S. Tagliapietra, *Beilstein J. Org. Chem.*, 2014, **10**, 1454–1461; (*c*) C. O. Kappe, B. Pieber and D. Dallinger, *Angew. Chem., Int. Ed.*, 2013, **52**, 1088–1094.